To appear in *The Astrophysical Journal*.
Preprint typeset using LaTeX style emulateapj v. 26/01/00

ESTIMATING BLACK HOLE MASSES IN ACTIVE GALAXIES USING THE Hα EMISSION LINE

Jenny E. Greene
Harvard-Smithsonian Center for Astrophysics, 60 Garden St., Cambridge, MA 02138

and

Luis C. Ho
The Observatories of the Carnegie Institution of Washington, 813 Santa Barbara St., Pasadena, CA 91101

To appear in The Astrophysical Journal.

ABSTRACT

It has been established that virial masses for black holes in low-redshift active galaxies can be estimated from measurements of the optical continuum strength and the width of the broad Hβ line. Under various circumstances, however, both of these quantities can be challenging to measure or can be subject to large systematic uncertainties. To mitigate these difficulties, we present a new method for estimating black hole masses. From analysis of a new sample of broad-line active galactic nuclei, we find that Hα luminosity scales almost linearly with optical continuum luminosity and that a strong correlation exists between Hα and Hβ line widths. These two empirical correlations allow us to translate the standard virial mass system to a new one based solely on observations of the broad Hα emission line.

Subject headings: galaxies: active — galaxies: jets — galaxies: nuclei — galaxies: Seyfert — quasars: general

1. INTRODUCTION

The recent discovery of a tight correlation between black hole (BH) mass and the stellar velocity dispersion of the bulge of the host galaxy (the $M_{\rm BH}-\sigma_*$ relation; Gebhardt et al. 2000a; Ferrarese & Merritt 2000) has sparked renewed interest in deriving BH masses in active galactic nuclei (AGNs). Reverberation mapping (e.g., Blandford & McKee 1982) experiments can yield estimates of the radius of the broad-line region (BLR) from the lag between the variability in the AGN continuum and the corresponding variability in the broad permitted lines. With the BLR radius ($R_{\rm BLR}$) in hand and some measure of the BLR velocity dispersion (v), one can infer a virial mass for the BH, $M_{\rm BH}=v^2R_{\rm BLR}/G$ (Ho 1999; Wandel, Peterson, & Malkan 1999; Kaspi et al. 2000). Remarkably, this simple prescription yields BH masses that seem to be accurate to a factor of $\sim$3 when compared against the $M_{\rm BH}-\sigma_*$ relation (Gebhardt et al. 2000b; Ferrarese et al. 2001; Nelson et al. 2004; Onken et al. 2004). The number of AGNs with BH masses derived from reverberation mapping is currently small (35), but $M_{\rm BH}$ can be estimated indirectly from single-epoch spectra using an empirical correlation between $R_{\rm BLR}$ and optical continuum luminosity that has been calibrated using the reverberation-mapped sample: $R_{\rm BLR}\propto L_{5100}^{0.7}$ (Kaspi et al. 2000), where $L_{5100}=\lambda L_\lambda$ at $\lambda=5100$ Å. From a single-epoch spectrum one can measure both v and L_{5100}, and thereby infer $M_{\rm BH}$.

While virial estimates of BH masses have been widely used in the literature (e.g., Vestergaard 2002; Greene & Ho 2004), various systematic uncertainties may affect the measurements of both luminosity and velocity. Broad Fe II emission in Type 1 AGNs can add ambiguity in the determination of the optical continuum luminosity at 5100 Å. In lower-luminosity AGNs, dilution by host galaxy starlight can be so severe that it becomes very difficult, if not virtually impossible, to isolate the nonstellar continuum unambiguously. As noted by Wu et al. (2004), an additional complication arises in sources, such as blazars, whose optical continuum can be subject to contamination by synchrotron emission from jets, which might be partly beamed. Under these circumstances, the observed L_{5100} overestimates the true thermal component that governs the BLR size-luminosity relation.

For nearby AGNs, including the primary reverberation-mapped sample (Kaspi et al. 2000), the velocity dispersion used in the virial expression is usually measured through the width of the broad Hβ line. However, Hβ is at least a factor of 3 weaker than Hα, and so from considerations of signal-to-noise ratio (S/N) alone Hα, if available, is superior to Hβ. In practice, in some cases Hα may be the *only* detectable broad permitted line in the optical (traditionally such objects are known as Seyfert 1.9 galaxies; Osterbrock 1981).

In an effort to minimize uncertainties in virial BH mass estimates, and to broaden their applicability to classes of AGNs that would otherwise be inaccessible using the conventional methodology (e.g., blazars, galaxy-dominated low-luminosity sources, Type 1.9 Seyferts), we propose to translate the virial mass system of Kaspi et al. (2000), which makes use of the 5100 Å continuum luminosity and the broad Hβ line width, to a new system based *entirely* on observations of the broad Hα line. We achieve this in two steps. First, we revisit the well-known empirical correlation between optical continuum luminosity and Balmer emission-line luminosity (Yee 1980; Shuder 1981; Ho & Peng 2001), which now can be established with much greater precision using large, homogeneous samples of AGNs. This allows us to replace L_{5100} with $L_{\rm H\alpha}$, which has the advantage of being relatively straightforward to measure even for low-luminosity or galaxy-dominated sources (e.g., Ho et al. 1997; Greene & Ho

2004). Unlike the optical continuum, the line emission is also expected to be little affected by the jet component in radio-loud sources or blazars (e.g., Wang, Ho, & Staubert 2003). This approach is similar to that taken by Wu et al. (2004), who converted L_{5100} to $L_{\mathrm{H}\beta}$, but their analysis was confined to the original reverberation mapping sample of Kaspi et al. (2000), which consists, by necessity, of AGNs that are variable on timescales probed by current reverberation mapping experiments. This selection effect may result in subtle biases, and, in any case, the sample suffers from limited statistics. Secondly, we substitute the line width of Hβ with that of Hα, using a newly derived empirical correlation between the two.

Throughout we assume the following cosmological parameters to calculate distances: $H_0 = 100h = 71$ km s^{-1} Mpc^{-1}, $\Omega_{\mathrm{m}} = 0.27$, and $\Omega_\Lambda = 0.75$ (Spergel et al. 2003).

2. THE SAMPLE

We utilize the large and homogeneous database provided by the Sloan Digital Sky Survey (SDSS; York et al. 2000), which will eventually obtain imaging and follow-up spectroscopy for about one-quarter of the sky. Briefly, spectroscopic candidates are selected based on multi-band imaging (Strauss et al. 2002) with a drift-scan camera (Gunn et al. 1998). A pair of spectrographs is fed by 3″-diameter fibers, covering $\sim 3800 - 9200$ Å with an instrumental resolution of $\lambda/\Delta\lambda \approx 1800$ (Gaussian $\sigma_{\mathrm{inst}} \approx 71$ km s^{-1}). Integration times are determined for a minimum S/N = 4 at $g = 20.2$ mag. The spectroscopic pipeline performs basic image calibrations, as well as spectral extraction, sky subtraction, removal of atmospheric absorption bands, and wavelength and spectrophotometric calibration (Stoughton et al. 2002). Finally, spectral classification is performed using cross-calibration with stellar, emission-line, and active galaxy templates. The Third Data Release (DR3; Abazajian et al. 2005) of SDSS contains 45,260 spectroscopically identified AGNs with $z < 2.3$. Of these, ~ 3000 have $z \leq 0.35$, and hence Hα in the bandpass.

From this sample we select objects with a high S/N (≥ 25 per pixel) and low galaxy contamination, so that we can unambiguously measure L_{5100}. We use the equivalent width (EW) of the Ca II K λ3934 line to estimate the degree of galaxy contamination; within the SDSS bandpass this is the highest-EW stellar absorption feature that is not confused with line emission. By artificially diluting composite galaxy spectra[1] from Bernardi et al. (2003) with varying levels of featureless AGN continuum (which for a narrow spectral region is well approximated by a constant), we find that an EW cutoff of 1.5 Å for the Ca II K line corresponds to a galaxy contribution of $\leq 20\%$. Thus, our primary sample was chosen to satisfy EW(Ca K) ≤ 1.5 Å. In order to increase the dynamic range of the sample at the lowest luminosities, we included ~ 30 more galaxies, including the 19 objects from Greene & Ho (2004), which have a mean S/N ≈ 17 and EW(Ca K) as high as 10 Å. The total sample consists of 229 objects.

To investigate the possible influence of jet emission on L_{5100}, we also consider an auxiliary sample of 59 radio-loud objects, selected using the standard criterion for radio-loudness, $R \geq 10$, where R is the ratio of the flux densities at 6 cm and 4400 Å (Kellermann et al. 1989). The radio flux densities were obtained from the Faint Images of the Radio Sky at Twenty-cm (FIRST; Becker, White, & Helfand 1995) survey, which covers all the objects in our sample. We corrected the flux densities from 20 cm to 6 cm assuming a spectrum $f_\nu \propto \nu^{-0.46}$ (Ho & Ulvestad 2001). The derived R values for the radio-loud sample range from 10 to 10^4.

3. SPECTRAL FITTING

Below we discuss our method to measure the AGN continuum and the broad emission lines. The continuum and line measurements are corrected for Galactic extinction using the extinction map of Schlegel, Finkbeiner, & Davis (1998) and the reddening law of Cardelli, Clayton, & Mathis (1989).

3.1. *Continuum*

The nonstellar, featureless continuum of Type 1 (broad-line) AGNs is challenging to measure at optical wavelengths because it is entangled with a complex emission-line spectrum and starlight, depending on the relative brightness of the nucleus with respect to the host galaxy. Particularly troublesome are the broad, blended Fe II multiplets, which form a "pseudo-continuum" that litters most of the spectrum, but especially the regions flanking Hβ. Moreover, the intrinsic shape of the featureless continuum itself is not well known. For the objects that have minimal starlight contamination, which, by selection, constitute the majority of our sample, we decompose the spectrum by simultaneously fitting a two-component model consisting of (1) an underlying featureless continuum and (2) an empirical Fe II template. In practice, the featureless continuum over the optical region can be approximated well by a double power law, with a spectral break at $\lambda \approx 5000$ Å (Vanden Berk et al. 2001; M. Kim & L. C. Ho 2005, in preparation). We require that the combined flux of the two power-law components at 5600 Å, a relatively line-free region, be equal to the observed flux at that point. Following Boroson & Green (1992), an effective Fe II template can be generated by a simple velocity-broadening and scaling of the Fe II spectrum derived from observations of the "narrow-line" Type 1 AGN I Zw 1 (kindly provided by T. Boroson). In order to avoid contamination from strong spectral lines, we only include the following regions in our fit: 4170–4260, 4430–4770, 5080–5550, 6050–6200, and 6890–7010 Å. We do not fit the region below 3685 Å, since it is not covered by the I Zw 1 Fe II template of Boroson & Green (1992); consequently, we do not have to model the Balmer continuum (e.g., Wills, Netzer, & Wills 1985).

Approximately 30 objects at the lowest luminosities have sufficient galaxy contamination to warrant removing it. In lieu of more sophisticated methods for starlight decomposition (e.g., Greene & Ho 2004, 2005), we find that for the present sample the galaxy continuum can be modeled adequately using a scaled spectrum of a velocity-broadened K giant star (obtained from the SDSS).

[1]The composite spectra are constructed from a library of ~ 9000 early-type galaxies from SDSS, and span a wide range in velocity dispersion, redshift, luminosity, and effective radius. We degrade the S/N ratio of the composites to match that of our sample.

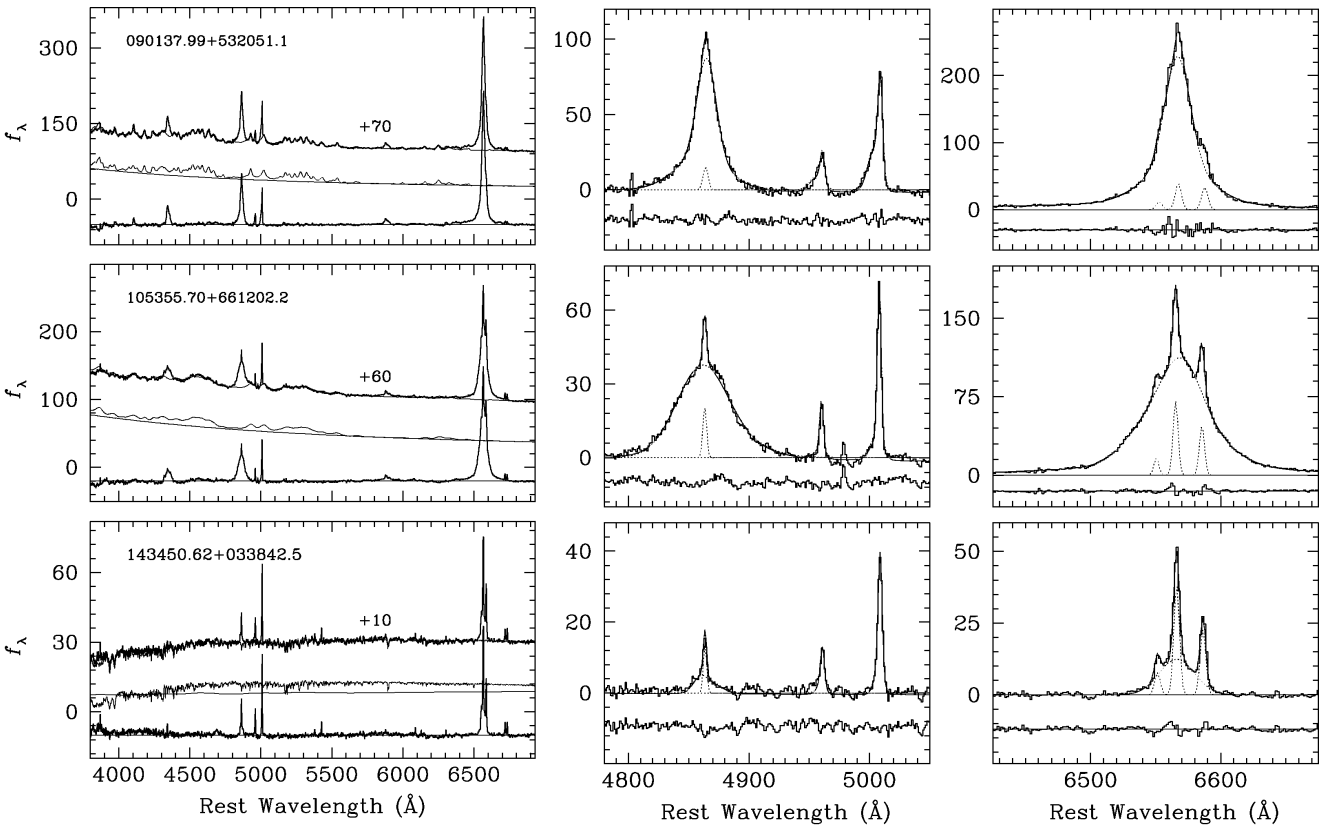

FIG. 1.— Sample spectra for three objects in our sample. The ordinate is in units of 10^{-17} erg s^{-1} cm^{-2} Å^{-1}. *Left*: In each panel, the top shows the observed spectrum overplotted with the model for the continuum, offset in the ordinate for clarity. The middle shows the fitted components (power law, Fe II template, and, if necessary, host galaxy) of the continuum model, with no offset. The bottom shows the continuum-subtracted, emission-line spectrum. *Center*: Fits to the Hβ+[O III] $\lambda\lambda$4959, 5007 region. The data are shown in histogram, the fitted broad and narrow components are shown in dotted lines, and the final model (sum of all components) is shown as a solid line. The residuals are plotted below. *Right*: Same as the middle panels, but for the Hα+[N II] $\lambda\lambda$6548, 6583 complex.

3.2. *Emission Lines*

The primary challenge in measuring accurate fluxes and profiles of broad emission lines is to properly deblend contaminating narrow-line components. Here we are only concerned with the region immediately surrounding Hα and Hβ. For Hα, as outlined in Greene & Ho (2004; see also Ho et al. 1997), we begin by constructing a model for the narrow components using the [S II] $\lambda\lambda$6716, 6731 lines. In short, a multi-Gaussian model is fit to the [S II] doublet, and then shifted and scaled to fit the Hα+[N II] $\lambda\lambda$6548, 6583 complex. The relative positions of the narrow Hα and [N II] lines are constrained by their laboratory values, and the relative ratio of the two [N II] components is fixed to 2.96. We then fit the broad component of Hα with as many Gaussian components as needed to provide a statistically acceptable fit. This method provides the needed flexibility to reproduce highly non-Gaussian, asymmetric profiles, but we attach no physical significance to the individual components.

The fitting procedure for Hβ is similar to that outlined above; in this case the narrow-line contamination comes from the narrow component of Hβ and [O III] $\lambda\lambda$4959, 5007. Because of their proximity, we first experimented with modeling the narrow Hβ component using [O III] as a template, but could not reliably obtain a satisfactory fit. The mismatch stems partly from the frequently observed asymmetric blue wing of [O III] (Greene & Ho 2005)[2]. The profile of [O III] is also expected to be a poor representation of the profile of [S II] (and hence narrow Hα and Hβ) if the narrow-line region is stratified in density (see discussion in Greene & Ho 2005). Therefore, as with Hα, we use the template built from [S II] to model narrow Hβ. The Hβ centroid is fixed relative to the narrow Hα position while its flux is limited by the value appropriate for Case B′ recombination (Hα = 3.1 Hβ; Osterbrock 1989). We simultaneously fit [O III] using a two-component Gaussian (identical for both lines of the doublet), one for the core and another for the blue wing, as described in Greene & Ho (2005). Finally, the broad Hβ profile is modeled as a multi-component Gaussian, analogous to Hα. While in general we find that this procedure provides an acceptable fit to the entire region, there were some cases ($\sim$ 20) for which we could not obtain an acceptable fit for the narrow Hβ using the [S II] model; this may be due to gross variations in spectral resolution between the blue and red ends of the spectrum. In these cases, in order to fit the narrow Hβ component, we retain the flux and centroid limits described above but relax the line width constraint, and instead impose an (rather arbitrary) upper limit of $\sigma \leq 550$ km s^{-1}.

3.3. *Errors and Uncertainties*

In objects with minimal galaxy contamination, the uncertainty in the flux of the optical continuum is dominated

[2]The blue asymmetric wing of [O III] is presumably absent from the narrow component of Hα and Hβ, since [S II], which generally lacks the asymmetric component (Greene & Ho 2005), fits Hα well.

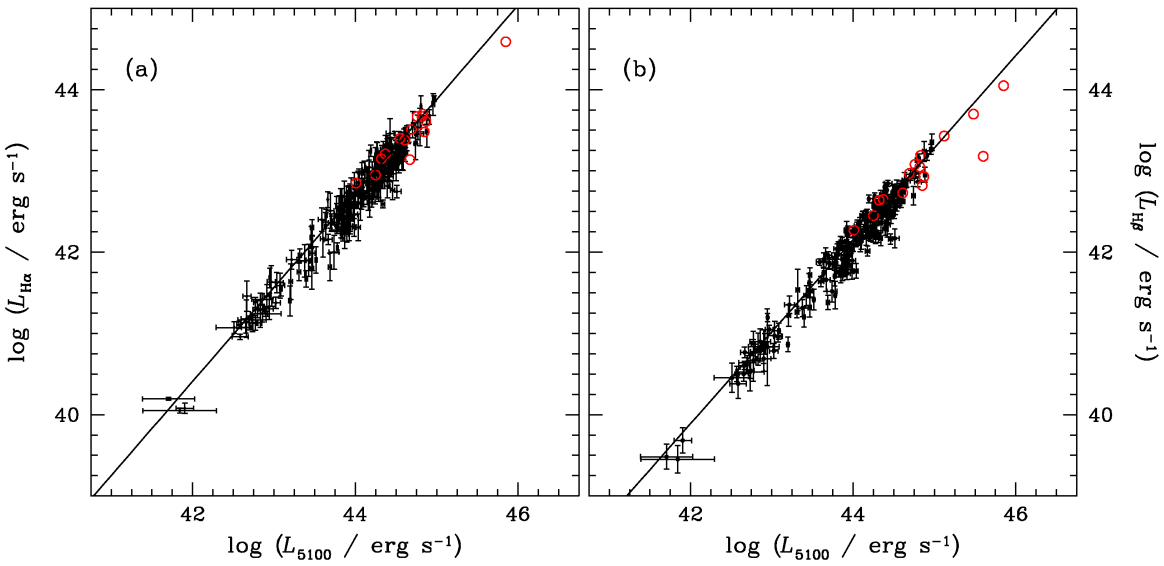

FIG. 2.— The correlation between L_{5100} and (*a*) $L_{H\alpha}$ and (*b*) $L_{H\beta}$ for the combined broad and narrow components of the line. Filled points are our measurements, and open (red) points are from Kaspi et al. (2000). The error bars for the points from Kaspi et al. are smaller than the symbol size. The line gives the ordinary least-squares fit to the data.

by the proper removal of Fe II emission and errors in the continuum slope. We use the measured Fe II flux at 5100 Å to estimate the uncertainty contributed by our decomposition. To estimate errors resulting from the power-law fit, we average the fluxes obtained when the slope of the power law is allowed to increase or decrease by one standard deviation, as obtained from the fit. The final adopted error is the quadrature sum of the Fe II and slope errors, although the latter usually dominates. Typical errors are $\sim$ 0.04 dex. The largest source of uncertainty in measurements of line flux comes from the placement of the continuum level. We estimate our uncertainty by adjusting the continuum level by one standard deviation above and below the nominal best-fit level of the continuum, and then recalculating the line flux. Typical errors in the flux are $\sim$ 35%, or 0.13 dex.

Estimating errors in line width is more difficult, since uncertainty in the decomposition between broad and narrow components dominates the measurement error. In some cases the separation is obvious, but in others (see, e.g., the top panel of Fig. 1) there is no clear distinction between the two components. We generate an artificial spectrum for each object by combining the best-fit model emission lines and Gaussian random errors with matching S/N. An artificial spectrum generated in this manner will suffer from the same decomposition ambiguity as the original data. We then fit these artificial spectra using our fitting procedure, as outlined above. The estimated uncertainty is simply taken to be the difference between the model and measured FWHM. We find that S/N significantly impacts the reliability of our fits. While typical errors are $\sim$ 7% (or 0.03 dex) and $\sim$ 10% (0.05 dex) for FWHM$_{H\alpha}$ and FWHM$_{H\beta}$, respectively, these are found to increase to as much as 0.1 dex in cases with the lowest S/N.

4. RESULTS

4.1. *Empirical Correlations*

Our data reveal a well-defined correlation between Balmer emission-line luminosity and L_{5100}. This is illustrated in Figure 2, which includes the reverberation-mapped sample from Kaspi et al. (2000). Treating L_{5100} as the independent variable (under the assumption that L_{5100} traces the continuum that powers the line emission) and accounting for errors in both variables (Press et al. 1992), an ordinary least-squares fit yields

$$L_{H\alpha} = (5.25\pm0.02)\times10^{42}\left(\frac{L_{5100}}{10^{44}\ \mathrm{erg\ s^{-1}}}\right)^{(1.157\pm0.005)}\ \mathrm{erg\ s^{-1}} \quad (1)$$

and

$$L_{H\beta} = (1.425\pm0.007)\times10^{42}\left(\frac{L_{5100}}{10^{44}\ \mathrm{erg\ s^{-1}}}\right)^{(1.133\pm0.005)}\ \mathrm{erg\ s^{-1}}. \quad (2)$$

The rms scatter in the above luminosity-luminosity relations is quite small, being only $\sim$ 0.2 dex in each case. The correlation strengths are correspondingly strong, with Kendall's $\tau = 0.8$, and do not improve when FWHM is included as a third parameter using the partial correlation test of Akritas & Siebert (1996). These relations are fit for the combined broad and narrow components. However, the best-fit parameters are virtually unchanged when only the broad component is considered, since the narrow component accounts for only $\sim$ 7% and $\sim$ 10% of the total Hα and Hβ flux, respectively. Note that the slopes of both correlations are formally larger than unity, which

can be excluded at a confidence level of $> 99\%$ based on bootstrap simulations.

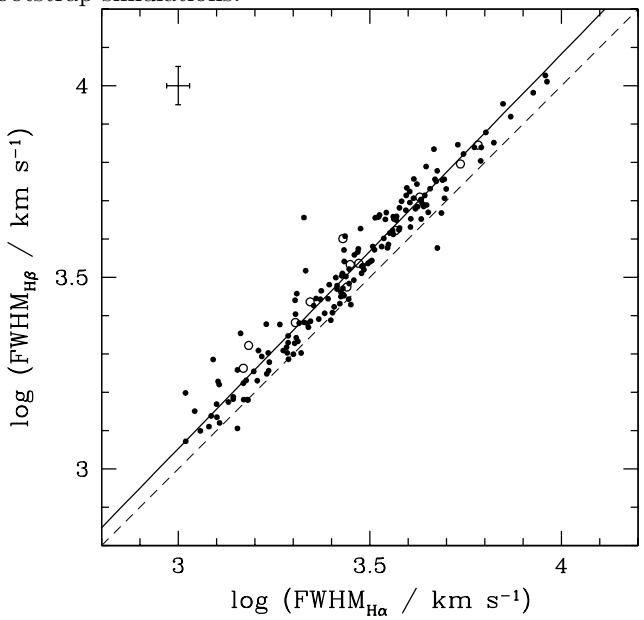

FIG. 3.— The correlation between Hα and Hβ line widths. Filled points are our measurements, and open points are from Kaspi et al. (2000). The solid line gives the ordinary least-squares fit to the 162 objects with EW(Hβ) > 50 Å. The dashed line denotes FWHM$_{H\alpha}$ = FWHM$_{H\beta}$. A typical error bar is shown in the top-left corner.

We also find a well-defined correlation between the Hα and Hβ line width (Fig. 3), which we parameterize[3] by the FWHM. In this case, neither FWHM$_{H\alpha}$ nor FWHM$_{H\beta}$ can be regarded as the independent variable, so we calculate the ordinary least-squares bisector, again accounting for errors in both parameters (Akritas & Bershady 1996). Whereas for the line-continuum correlations we were forced to include lower-S/N spectra in order to increase the dynamic range in luminosity, in this case we can span the entire range in line width without considering the full sample. To minimize errors resulting from profile decomposition, we concentrate on spectra with strong Hβ lines by excluding objects with Hβ EWs less than 50 Å. For this restricted sample of 162 objects, we find

$$\mathrm{FWHM_{H\beta}} = (1.07\pm0.07)\times10^3 \left(\frac{\mathrm{FWHM_{H\alpha}}}{10^3\ \mathrm{km\ s^{-1}}}\right)^{(1.03\pm0.03)} \mathrm{km\ s^{-1}} \quad (3)$$

The rms scatter around the best-fit line is ~ 0.1 dex. We note that when we include the entire sample, or look at the radio-loud subset separately, Hβ is still on average broader than Hα, but the scatter is larger and the slope of the correlation changes slightly.

4.2. *Radio-loud Sources*

If the optical continuum of radio-loud sources is significantly boosted by nonthermal emission from a jet, their L_{5100}, and hence virial mass, will be systematically overestimated. We can empirically test the magnitude of this effect by examining the correlation between L_{5100} and Balmer-line luminosity for our auxiliary radio-loud sample. If jet contamination is important, we would expect the

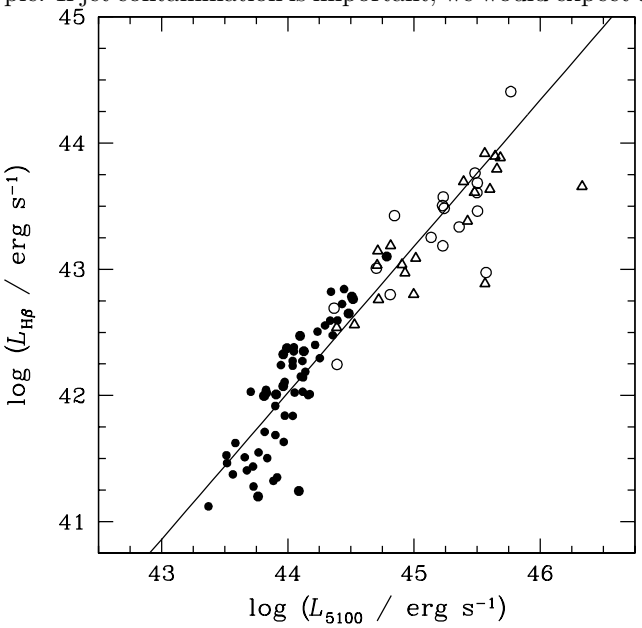

FIG. 4.— The correlation between L_{5100} and $L_{H\beta}$ luminosity (broad + narrow components) for the radio-loud sources. Filled symbols are from our sample; open symbols are from Brotherton (1996). Core-dominated sources with core-to-lobe luminosity ratios ≥ 1 are marked as triangles. The line represents our best fit to the $L_{H\beta}$-L_{5100} relation shown in Figure 2*b*.

radio-loud objects to lie systematically to the right of the best-fit relations shown in Figure 2. However, as shown in Figure 4, the radio-loud sources (filled points) do not show a significant offset with respect to the main sample. Their mean displacement from our best-fit $L_{H\beta}$-L_{5100} line is only $+0.02$ dex in L_{5100}, and for the strongest radio sources ($R \geq 100$) the mean displacement is in fact -0.04; neither result is statistically significant. Instead of the degree of radio-loudness, the more important parameter may be the amount of beaming, which can be guaged roughly by the degree of core dominance of the radio emission. Unfortunately, the resolution of FIRST ($5''$ or 10 kpc at $z = 0.1$) is inadequate to distinguish truly core-dominated objects from objects with intrinsically compact jets. We thus additionally consider objects from the sample of Brotherton (1996), which is composed entirely of radio-loud objects with tabulated core-to-lobe radio luminosity ratios. For the 37 Brotherton objects with measured V-band magnitudes and R values, we calculate L_{5100} assuming an intrinsic AGN continuum spectrum of $f_\nu \propto \nu^{-0.45}$ (Vanden Berk et al. 2001). Brotherton's sample is, on average, about an order of magnitude more luminous than ours. The entire Brotherton sample (open symbols in Fig. 4) is displaced by $+0.1$ dex from the fiducial line of radio-quiet objects, increasing to $+0.14$ dex for the core-dominated systems (defined as those with core-to-lobe ratios ≥ 1; open triangles). We conclude that BH masses based on L_{5100} can be systematically overestimated in radio-loud objects, but the effect is only serious for relatively luminous, core-dominated sources. While the systematic enhancement

[3]Peterson et al. (2004) advocate the use of the actual line dispersion (second moment of the line profile). We have adopted the FWHM here for consistency with the formalism of Kaspi et al. (2000). We also find that the empirical correlation between the line widths of Hα and Hβ is significantly tighter using FWHM than the line dispersion.

of the optical continuum relative to Balmer line emission in the most radio-loud, core-dominant sources can be attributed reasonably to jet contamination, we cannot rule out the possibility that this effect is due to changes in the ionizing spectrum or covering factor of the line-emitting gas.

4.3. *A New Formalism for Estimating BH Virial Masses*

The existence of the tight empirical correlations described above (Eqs. 1 and 3) implies that we can transform the virial mass expression of Kaspi et al. (2000), which makes use of L_{5100} and $\mathrm{FWHM_{H\beta}}$, into a new formalism that depends solely on the observed properties of the broad Hα line (namely $L_{\mathrm{H}\alpha}$ and $\mathrm{FWHM_{H\alpha}}$, derived from a single-epoch spectrum), without incurring appreciable additional uncertainty.

We begin by rederiving the radius-luminosity relation of Kaspi et al. (2000), using the more recent Hβ lags (derived from the cross-correlation centroid) and L_{5100} luminosities listed in Peterson et al. (2004), corrected to our adopted cosmology. The data points that Peterson et al. deem to be uncertain are omitted. We calculate symmetric error bars using the mean of the quoted upper and lower uncertainties, and use the weighted average of all available lag measurements. Using an ordinary least-squares fit with uncertainties in both parameters, we obtain

$$R_{\mathrm{BLR}} = (30.2 \pm 1.4) \left(\frac{L_{5100}}{10^{44}\ \mathrm{erg\ s^{-1}}}\right)^{0.64\pm0.02} \mathrm{lt-days}. \quad (4)$$

Note that the slope of the radius-luminosity relation, 0.64 ± 0.02, is somewhat shallower than that originally published by Kaspi et al. (2000), 0.700 ± 0.033, although it is consistent with the value of 0.67 ± 0.07 recently rederived by Kaspi et al. (2005). For $v = \frac{\sqrt{3}}{2}\ v_{\mathrm{FWHM}}$, appropriate for random orbits, and using $v_{\mathrm{FWHM}} = \mathrm{FWHM_{H\beta}}$ for consistency with Kaspi et al. (2000), the virial formula[4] for BH mass is

$$M_{\mathrm{BH}} = (4.4 \pm 0.2) \times 10^6 \left(\frac{L_{5100}}{10^{44}\ \mathrm{erg\ s^{-1}}}\right)^{0.64\pm0.02} \left(\frac{\mathrm{FWHM_{H\beta}}}{10^3\ \mathrm{km\ s^{-1}}}\right)^2 M_\odot. \quad (5)$$

Substituting Equations 1 and 3 into Equation 5, we obtain a virial mass formula that depends on the Hα line alone:

$$M_{\mathrm{BH}} = (2.0^{+0.4}_{-0.3}) \times 10^6 \left(\frac{L_{\mathrm{H}\alpha}}{10^{42}\ \mathrm{erg\ s^{-1}}}\right)^{0.55\pm0.02} \left(\frac{\mathrm{FWHM_{H\alpha}}}{10^3\ \mathrm{km\ s^{-1}}}\right)^{2.06\pm0.06} M_\odot. \quad (6)$$

While we argue that Hα is the line of choice whenever possible, we recognize that often Hβ is more readily available (for instance, due to redshift constraints). In such cases, it might still be preferable to use $L_{\mathrm{H}\beta}$ rather than L_{5100}, and for completeness we give the virial mass formula based only on the Hβ line:

$$M_{\mathrm{BH}} = (3.6 \pm 0.2) \times 10^6 \left(\frac{L_{\mathrm{H}\beta}}{10^{42}\ \mathrm{erg\ s^{-1}}}\right)^{0.56\pm0.02} \left(\frac{\mathrm{FWHM_{H\beta}}}{10^3\ \mathrm{km\ s^{-1}}}\right)^2 M_\odot. \quad (7)$$

4.4. *Comparison with Kaspi et al. (2005)*

Kaspi et al. (2005) revisit the radius-luminosity relation for the reverberation-mapped sample, and we present a brief comparison of our respective results. Our best-fit R_{BLR}-L_{5100} slope, 0.64 ± 0.02, is consistent with the result of Kaspi et al., who find a best-fit slope of 0.67 ± 0.07 for R_{BLR} derived from Hβ lags alone (line 18 of their Table 3). The slight discrepancy between our value and theirs stems from a combination of the slightly differing cosmologies, samples, and fitting techniques employed in the two studies. For completeness, we recast our BH mass estimators based on the radius-luminosity relation of Kaspi et al. (2005):

$$R_{\mathrm{BLR}} = (20.0^{+2.8}_{-2.4}) \left(\frac{L_{5100}}{10^{44}\ \mathrm{erg\ s^{-1}}}\right)^{0.67\pm0.07} \mathrm{lt-days}. \quad (8)$$

Kaspi et al. (2005) consider a radius-luminosity relation derived from the average lags of all the Balmer lines, but we prefer to focus on the relation based exclusively on Hβ lags because the significant difference we find between the FWHMs of Hα and Hβ suggests that the lines form, at least in part, from kinematically and possibly spatially distinct regions. The resulting relations are

$$M_{\mathrm{BH}} = (1.3 \pm 0.3) \times 10^6 \left(\frac{L_{\mathrm{H}\alpha}}{10^{42}\ \mathrm{erg\ s^{-1}}}\right)^{0.57\pm0.06} \left(\frac{\mathrm{FWHM_{H\alpha}}}{10^3\ \mathrm{km\ s^{-1}}}\right)^{2.06\pm0.06} M_\odot. \quad (9)$$

$$M_{\mathrm{BH}} = (2.4 \pm 0.3) \times 10^6 \left(\frac{L_{\mathrm{H}\beta}}{10^{42}\ \mathrm{erg\ s^{-1}}}\right)^{0.59\pm0.06} \left(\frac{\mathrm{FWHM_{H\beta}}}{10^3\ \mathrm{km\ s^{-1}}}\right)^2 M_\odot. \quad (10)$$

Kaspi et al. also derive a new R_{BLR}-$L_{\mathrm{H}\beta}$ relation from the reverberation-mapped sample. Their slope of 0.69 ± 0.06 differs somewhat from the 0.56 ± 0.02 found here (Eq. 7). While the small difference in adopted cosmology plays some role, most of the discrepancy arises from the different luminosity ranges covered by our respective samples. Our Hβ luminosities range from $\sim 10^{39.5}$ to 10^{43} erg s^{-1}, whereas Kaspi et al.'s sample has very few points below 10^{41} erg s^{-1}. When use a restricted sample with $L_{\mathrm{H}\beta} > 10^{41}$ erg s^{-1}, we obtain a L_{5100}-$L_{\mathrm{H}\beta}$ relation with a shallower slope of 0.97 ± 0.04, which would lead to a steeper R_{BLR}-$L_{\mathrm{H}\beta}$ relation, consistent with that found by Kaspi et al.. A homogeneous sample covering as wide a

[4] By comparing reverberation mapping masses with an enlarged sample of bulge velocity dispersions, Onken et al. (2004) advocate a normalization factor for the virial formula larger than the one we adopted by a factor of 1.8.

luminosity range as possible is required to address the issue of whether the slope of the $R_{\rm BLR}$-$L_{\rm H\beta}$ relation is truly luminosity-dependent.

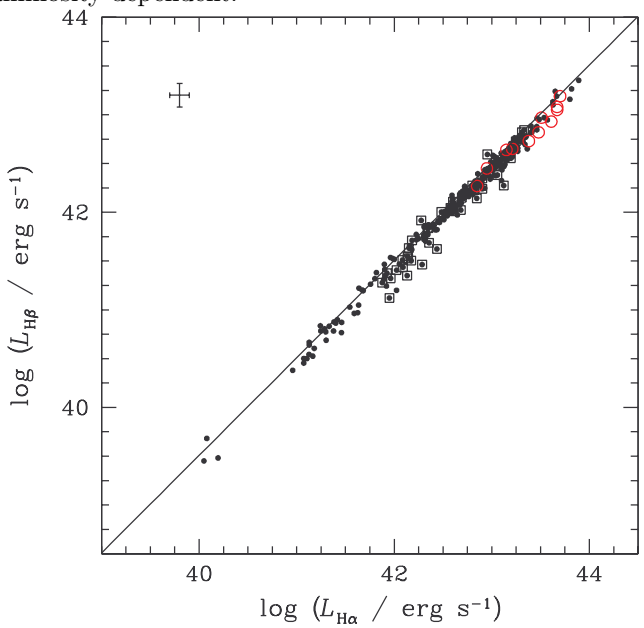

FIG. 5.— Correlation between $L_{\rm H\beta}$ and $L_{\rm H\alpha}$, for the combined broad and narrow components of the lines. Filled points are our measurements, and open (red) points are from Kaspi et al. (2000); radio-loud objects have boxes around them. The line represents $L_{\rm H\alpha} = 3.1\ L_{\rm H\beta}$, as expected for Case B′ recombination. The data follow this relation quite closely. A typical error bar is shown in the upper-left corner.

5. DISCUSSION

The new virial mass formalism based on the Hα emission line, which is ultimately calibrated against the mass scale of reverberation-mapped AGNs, relies on two strong empirical correlations presented in this paper. The first correlation, that between optical continuum luminosity and Balmer emission-line luminosity, has long been known (e.g., Yee & Oke 1978; Yee 1980). Shuder (1981) compiled many of the early measurements, spanning a wide range of Hα luminosity from $\sim 10^{40}$ to 10^{44} erg s^{-1}. He showed that $L_{\rm H\alpha}$ traces the optical continuum luminosity with a slope of 1.05 ± 0.03, consistent with unity and very similar to the slope found here (1.157 ± 0.005). Similarly, from an analysis of AGNs ranging from nearby low-luminosity Seyferts to quasars, Ho & Peng (2001) found that the luminosity of the broad Hβ line, from $\sim 10^{38}$ to 10^{44} erg s^{-1}, correlates strongly with the B-band continuum luminosity, roughly of the form $L_{\rm H\beta} \propto L_B^{0.9}$. While this slope is formally shallower than that found in our sample (1.133 ± 0.005), the measurements for the low-luminosity sources in the sample of Ho & Peng are also considerably more uncertain, making it difficult to judge the significance of the apparent discrepancy. Our study, based on a large, uniform, and modern data set, provides an important confirmation of the earlier results.

The correlation between the luminosity of the Balmer lines and the optical continuum arises naturally if the latter traces the low-energy tail of a featureless continuum that extends into the far-ultraviolet, which powers the line emission through photoionization. Indeed, quite early on this simple picture provided a natural explanation for the observed uniformity of the EW of the broad Hβ line in AGNs (Searle & Sargent 1968). Recall that the slopes of the Balmer line versus continuum luminosity relations (Eqs. 1 and 2) are formally steeper than unity (1.16 and 1.13 for Hα and Hβ, respectively). This implies that the line strength increases mildly with increasing luminosity [EW(Hα) $\propto {L_{5100}}^{0.16}$; EW(H$\beta$) $\propto {L_{5100}}^{0.13}$], which means that the Balmer lines show an *inverse* Baldwin effect (Baldwin 1977). While various studies have found a roughly linear relation between optical continuum luminosity and $L_{\rm H\beta}$ (e.g., Yee 1980; Shuder 1981; Boroson & Green 1992; Dietrich et al. 2002), Croom et al. (2002), consistent with our study, report a positive slope of EW(Hβ) $\propto {L_{5100}}^{0.19}$ using composite spectra constructed from the 2dF+6dF quasar survey. These apparently conflicting results may be attributable to the different luminosity coverage in the different studies. As discussed by Croom et al., the luminosity-dependent variation of the Balmer line strengths may indicate that the shape of the ionizing continuum changes systematically with luminosity. Another possibility is that the covering factor of the line-emitting gas depends on luminosity.

The second major empirical correlation presented in this study links the line widths of the Hα and Hβ lines. While a number of studies have investigated the relative differences in the profiles of the Hα and Hβ lines (e.g., Osterbrock & Shuder 1982; Shuder 1982, 1984; Crenshaw 1986; Stirpe 1991; Kollatschny 2003), ours considers by far the largest and most homogeneous sample to date. Consistent with previous studies, we find that Hβ generally has a slightly broader profile than Hα. We measure $\langle {\rm FWHM_{H\beta}}/{\rm FWHM_{H\alpha}} \rangle = 1.17$ with an error in the mean of 0.01 and an rms of 0.2. This value is, in fact, identical to the average value found by Osterbrock & Shuder (1982), but considering our order-of-magnitude increase in sample size this agreement must be fortuitous. The relative profile of Hα and Hβ depends on both the kinematic and ionization structure of the BLR, since Hβ is emitted preferentially in regions of higher density and/or higher ionization parameter than Hα (e.g. Osterbrock 1989). The tendency for the Hβ profile to be broader than Hα is not surprising if the density or ionization parameter of the BLR increases with decreasing radii.

Further insights into the physical conditions of the BLR may be gleaned from the Balmer decrements that come as a by-product of our analysis. The ratio of broad Hα to Hβ strengths has been found to vary quite significantly from the value of 3.1 predicted by Case B′ recombination. For instance, while Seyfert 1 galaxies have typical Hα/Hβ ratios of $\sim 3.5 - 5$ (Adams & Weedman 1975; Osterbrock 1977), in both broad-line radio galaxies and Seyfert 1.9 galaxies values as high as 7–10 are seen (Osterbrock 1981). Interestingly, we find $\langle {\rm H\alpha}/{\rm H\beta} \rangle = 3.5$ (for the combined broad and narrow components; Fig. 5), which is virtually identical to the value seen in the SDSS quasar composite spectrum of Vanden Berk et al. (2001). [The mean Hα/Hβ ratio for the radio-loud group is slightly higher ($\sim$4), but given the smaller sample, this is only a marginally significant difference.] Since this value is only mildly larger than the theoretical limit of 3.1, it implies that processes that enhance the Balmer decrement, such as collisional excitation or self-absorption (e.g., Netzer 1975), are generally

not that important. We can also place a stringent limit on the amount of internal reddening by dust: for an intrinsic Balmer decrement of 3.1, the extinction law of Cardelli et al. (1989) would allow at most $E(B-V) = 0.12$ mag. Most likely our selection of AGN-dominated sources has biased us against objects with large Balmer decrements, since the Balmer decrement may steepen in AGNs in the low state (e.g., Tran, Osterbrock, & Martel 1992; Korista & Goad 2004).

We will revisit the empirical correlations discussed above in a forthcoming study that considers a much larger and more statistically complete sample.

6. SUMMARY

We present a new method for estimating black hole masses from single-epoch optical spectra of AGNs, based entirely on the luminosity and line width of the broad Hα line. We achieve formal uncertainties comparable to those of the previous, widely used method of Kaspi et al. (2000) that relies on the AGN optical continuum luminosity and the width of the broad Hβ line. The advantage of our method is that it enables us to derive robust masses in objects where the AGN luminosity may be difficult (e.g., jet-dominated systems) or impossible (e.g., low-luminosity AGNs with significant galaxy contamination) to measure accurately, or in objects where the broad Hβ line may be missing altogether (e.g., Seyfert 1.9 galaxies). The robustness of the Hα-based mass estimator is due to two tight empirical correlations we have established: that between AGN optical continuum luminosity and Balmer emission-line luminosity on the one hand, and that between Hα and Hβ line width on the other. We briefly discuss some physical ramifications of these empirical correlations.

We thank T. Boroson for providing us with the I Zw 1 iron template and an anonymous referee for thoughtful comments that improved the manuscript. L. C. H. acknowledges support by the Carnegie Institution of Washington and by NASA grants from the Space Telescope Science Institute (operated by AURA, Inc., under NASA contract NAS5-26555). We are grateful to the SDSS collaboration for providing the extraordinary database and processing tools that made this work possible.

REFERENCES

Abazajian, K., et al. 2005, AJ, 129, 1755
Adams, T. F., & Weedman, D. W. 1975, ApJ, 199, 19
Akritas, M. G., & Bershady, M. A. 1996, ApJ, 470, 706
Akritas, M. G., & Siebert, J. 1996, MNRAS, 278, 919
Baldwin, J. A. 1977, ApJ, 214, 679
Becker, R. H., White, R. L., & Helfand, D. J. 1995, ApJ, 450, 559
Bernardi, M., et al. 2003, AJ, 125, 1882
Blandford, R. D., & McKee, C. F. 1982, ApJ, 255, 419
Boroson, T. A., & Green, R. F. 1992, ApJS, 80, 109
Brotherton, M. S. 1996, ApJS, 102, 1
Cardelli, J. A., Clayton, G. C., & Mathis, J. S. 1989, ApJ, 345, 245
Crenshaw, D. M. 1986, ApJS, 62, 821
Croom, S. M., et al. 2002, MNRAS, 337, 275
Dietrich, M., Hamann, F., Shields, J. C., Constantin, A., Vestergaard, M., Chaffee, F., Foltz, C. B., & Junkkarinen, V. T. 2002, ApJ, 581, 912
Ferrarese, L., Pogge, R. W., Peterson, B. M., Merritt, D., Wandel, A., & Joseph, C. L. 2001, ApJ, 555, L79
Ferrarese, L., & Merritt, D. 2000, ApJ, 539, L9
Gebhardt, K., et al. 2000a, ApJ, 539, L13
——. 2000b, ApJ, 543, L5
Greene, J. E., & Ho, L. C. 2004, ApJ, 610, 722
——. 2005, ApJ, in press (astro-ph/0503675)
Gunn, J. E., et al. 1998, AJ, 116, 3040
Ho, L. C. 1999, in Observational Evidence for Black Holes in the Universe, ed. S. K. Chakrabarti (Dordrecht: Kluwer), 157
Ho, L. C., Filippenko, A. V., Sargent, W. L. W., & Peng, C. Y. 1997, ApJS, 112, 391
Ho, L. C., & Peng, C. Y. 2001, ApJ, 555, 650
Ho, L. C., & Ulvestad, J. S. 2001, ApJS, 133, 77
Kaspi, S., Maoz, D., Netzer, H., Peterson, B. M., Vestergaard, M., Jannuzi, B. T. 2005, ApJ in press (astroph/0504484)
Kaspi, S., Smith, P. S., Netzer, H., Maoz, D., Jannuzi, B. T., & Giveon, U. 2000, ApJ, 533, 631
Kellermann, K. I., Sramek, R. A., Schmidt, M., Shaffer, D. B., & Green, R. F. 1989, AJ, 98, 1195
Kollatschny, W. 2003, A&A, 407, 461
Korista, K. T., & Goad, M. R. 2004, ApJ, 606, 749
Nelson, C. H., Green, R. F., Bower, G., Gebhardt, K., & Weistrop, D. 2004, ApJ, 615, 652
Netzer, H. 1975, MNRAS, 171, 395
Onken, C. A., Ferrarese, L., Merritt, D., Peterson, B. M., Pogge, R. A., Vestergaard, M., & Wandel, A. 2004, ApJ, 615, 645
Osterbrock, D. E. 1977, ApJ, 215, 733
——. 1981, ApJ, 249, 462
——. 1989, Astrophysics of Gaseous Nebulae and Active Galactic Nuclei (Mill Valley, CA: Univ. Science Books)
Osterbrock, D. E., & Shuder, J. M. 1982, ApJS, 49, 149
Peterson, B. M., et al. 2004, ApJ, 613, 682
Press, W. H., Teukolsky, S. A., Vetterling, W. T., & Flannery, B. P. 1992, Numerical Recipes, Second Ed. (Cambridge: Cambridge Univ. Press)
Schlegel, D. J., Finkbeiner, D. P., & Davis, M. 1998, ApJ, 500, 525
Searle, L., & Sargent, W. L. W. 1968, ApJ, 153, 1003
Shuder, J. M. 1981, ApJ, 244, 12
——. 1982, ApJ, 259, 48
——. 1984, ApJ, 280, 491
Spergel, D. N., et al. 2003, ApJS, 148, 175
Stirpe, G. M. 1991, A&A, 247, 3
Stoughton, C., et al. 2002, AJ, 123, 485
Strauss, M. A., et al. 2002, AJ, 124, 1810
Tran, H. D., Osterbrock, D. E., & Martel, A. 1992, AJ, 104, 2072
Vanden Berk, D. E., et al. 2001, AJ, 122, 549
Vestergaard, M. 2002, ApJ, 571, 733
Wandel, A., Peterson, B. M., & Malkan, M. A. 1999, ApJ, 526, 579
Wang, J.-M., Ho, L. C., & Staubert, R. 2003, A&A, 409, 887
Wills, B. J., Netzer, H., & Wills, D. 1985, ApJ, 288, 94
Wu, X.-B., Wang, R., Kong, M. Z., Liu, F. K., & Han, J. L. 2004, A&A, 424, 793
Yee, H. K. C. 1980, ApJ, 241, 894
Yee, H. K. C. , & Oke, J. B. 1978, ApJ, 226, 753
York, D. G., et al. 2000, AJ, 120, 1579